



Magnetic micro-manipulations to probe the local physical properties of porous scaffolds and to confine stem cells

Damien Robert^a, Delphine Fayol^a, Catherine Le Visage^b, Guillaume Frasca^a, Séverine Brulé^{b,c}, Christine Ménager^c, Florence Gazeau^a, Didier Letourneur^b, Claire Wilhelm^{a,*}

^aLaboratoire Matière et Systèmes Complexes (MSC), UMR 7057 CNRS & Université Paris Diderot, Paris, France

^bINSERM, U698, Bio-ingénierie Cardiovasculaire, Université Paris Diderot, CHU X. Bichat, Paris, France

^cUniv Paris 06-CNRS-ESPCI Laboratoire PECSA UMR7195, Paris, France

ARTICLE INFO

Article history:

Received 5 October 2009

Accepted 3 November 2009

Available online 24 November 2009

Keywords:

Tissue engineering

Porous scaffolds

Cell seeding

Mechanical properties

Magnetic tweezer

Iron oxide nanoparticles

ABSTRACT

The in vitro generation of engineered tissue constructs involves the seeding of cells into porous scaffolds. Ongoing challenges are to design scaffolds to meet biochemical and mechanical requirements and to optimize cell seeding in the constructs. In this context, we have developed a simple method based on a magnetic tweezer set-up to manipulate, probe, and position magnetic objects inside a porous scaffold. The magnetic force acting on magnetic objects of various sizes serves as a control parameter to retrieve the local viscosity of the scaffolds internal channels as well as the stiffness of the scaffolds pores. Labeling of human stem cells with iron oxide magnetic nanoparticles makes it possible to perform the same type of measurement with cells as probes and evaluate their own microenvironment. For 18 μm diameter magnetic beads or magnetically labeled stem cells of similar diameter, the viscosity was equivalently equal to 20 mPa s in average. This apparent viscosity was then found to increase with the magnetic probes sizes. The stiffness probed with 100 μm magnetic beads was found in the 50 Pa range, and was lowered by a factor 5 when probed with cells aggregates. The magnetic forces were also successfully applied to the stem cells to enhance the cell seeding process and impose a well defined spatial organization into the scaffold.

© 2009 Elsevier Ltd. All rights reserved.

1. Introduction

The field of tissue engineering has attracted much interest in the past decade with promises for successful therapeutic strategies in regenerative medicine to repair the loss of tissue or its function [1]. One of the fundamental techniques for the generation of tissue substitutes typically starts in vitro with the seeding of cells into porous scaffolds [2]. The scaffolds provide a three-dimensional (3-D) structure to support cell adhesion, migration, proliferation and finally tissue organization. Scaffolds are now being incorporated with stem cells for their ability to differentiate inside scaffolds or in the targeted tissue after implantation [3,4]. Biological and chemical attributes of scaffolds (biocompatibility, degradability, low toxicity, mediation of cell adhesion, etc.) as well as scaffolds morphology (architecture, porosity, etc.) play a fundamental role in the outcome of the cell seeding process [5–9]. Other requirements for successful cell seeding include the supply of a large number of

cells into scaffolds, an efficient attachment of the cells to the scaffold internal pores and the favorable environment to allow cell differentiation.

To improve the seeding density, a most common way is to use a bioreactor [10–12]. Recently, methods such as incorporation of cells as patches [13] or magnetic seeding [14,15] have been reported. The former method involves the use of a magnetic force to attract and retain the cells within the scaffolds, and combines the advantage of simplicity, rapidity and low cost. Magnetic force achieved to promote an efficient uniform distribution of cells inside the scaffolds but has not been investigated to control the cell organization in order to facilitate a more tissue-like structure. To date, no other techniques have yet demonstrated the ability to modulate cell organization into already formed 3-D porous scaffolds.

An efficient scaffold cellularization also requires the correct environment for cell adhesion and differentiation. On two-dimensional (2-D) model substrates, physical signals sensed by cells, such as matrix mechanical properties (local stiffness, adhesiveness, architecture, etc.) or the dynamics of the surrounding medium (shear stress, compression, etc.), are increasingly emerging as determinants of cell adhesion, migration and differentiation

* Corresponding author. Fax: +33 1 5727 6211.

E-mail address: claire.wilhelm@univ-paris-diderot.fr (C. Wilhelm).

Table 1

Magnetic probes used in the study: magnetic beads or magnetically labeled cells of diameter d (μm) and magnetic moment M in a 145 mT field (A m^2). The force $F_{1\text{mm}}$ exerted on each probe when 1 mm distant from the tip varies in the pN–nN range. The average apparent viscosity η_{app} (mPa s) and stiffness G_{app} (Pa) are indicated.

Probes	d (μm)	M (A m^2)	F_{tip}	$F_{1\text{mm}}$	η_{app} (mPa.s)	G_{app} (Pa)
Magnetic beads	4.6	1.8×10^{-13}	62 pN	11 pN	5.9 ± 4.2	–
Magnetic beads	18	4.9×10^{-12}	1.7 nN	304 pN	20.7 ± 15.3	–
Magnetic beads	100 ± 67	5.1×10^{-9}	1744 nN	316 nN	–	70.8 ± 15.1
Mesenchymal stem cells MSC	18 ± 4.2	1.3×10^{-12}	445 pN	81 pN	34.7 ± 23.9	–
Endothelial progenitor cells EPC	13.8 ± 2.1	6.6×10^{-13}	226 pN	41 pN	26.7 ± 19.1	–
Aggregates of EPC	80 ± 14	1.3×10^{-10}	45 nN	8 nN	273 ± 212	8.4 ± 7.4

[16–23]. It is now established that the mechanical microenvironment will be essential for the successful engineering of 3-D scaffolds to provide an appropriate support for cells [24,25]. When designing 3-D scaffolds for tissue engineering, the mechanical properties of the material have thus to be thoroughly investigated. The characterization of the microarchitecture at a micrometric scale, matching the cellular level, is essential prior achieving cell seeding in the scaffolds. This, in turn, will require accurate methods to measure mechanical properties at a microscale.

Macroscopic mechanical properties of scaffolds are mostly performed by tensile tests, compression tests, and dynamic mechanical analysis [22,26–28]. The local differences in the mechanical properties will not be detected by these bulk measurements. Atomic Force Microscopy (AFM) allows the assessment of the local physical properties [29,30] but probes only the material surface. Magnetic Resonance Elastography (MRE) technique is emerging to visualize spatial changes in mechanical properties [31]. Microscopic MRE has very recently been developed to provide a microscopic resolution of tenth of microns and applied to retrieve the shear stiffness of engineered constructs [32]. However, the need of magnetic resonance imaging (MRI) equipment together with high spatial resolution makes this pioneering technique still far to be routinely used in tissue engineering. Therefore, there is still a lack of methods for measuring the local microscopic mechanical properties inside 3-D scaffolds. Microrheology, based on the analysis of embedded particle motion, has emerged during the last decades as an experimental tool for picturing the mechanical properties of complex materials [33,34].

More recently, microrheology has been extended to precisely characterize the mechanical properties and heterogeneities of biomaterials [35,36] and living cells [37], at the microscopic scale. The most common microrheological approach consists in manipulating microbeads embedded in the material and recording their mechanical response. The beads motion can be imposed either by optical laser tweezers [38,39] or by magnetic tweezers [40]. The magnetic approach allows exerting forces at a distance, with no damage to the probed material. To our knowledge, such magnetic microbead rheology has not yet been applied to probe deeply, at a very local scale, the mechanics of porous scaffolds designed for tissue engineering. Finally, it becomes challenging not only to probe the scaffold physical properties with microbeads but also with the cells themselves in their 3-D environment.

Here we propose to develop the use of magnetic field gradients to manipulate, probe, and position magnetic objects inside scaffolds. The overall goal is to improve the potential of engineered tissue templates by controlling the cell seeding and characterizing locally the mechanical properties of the internal scaffold architecture. We have recently developed an efficient magnetic cell labeling with anionic magnetic iron oxide nanoparticles [41]. The labeling method has already been tested on a large number of cell types from different species, in primary cultured cells and cell lines, including immune cells, malignant cells, muscle cells, etc. The labeling did not affect cell proliferation, or the therapeutic and functional properties of the tested cell types, either in vitro or in vivo. These magnetic cellular nano-markers allow exerting magnetic forces on the labeled cells.

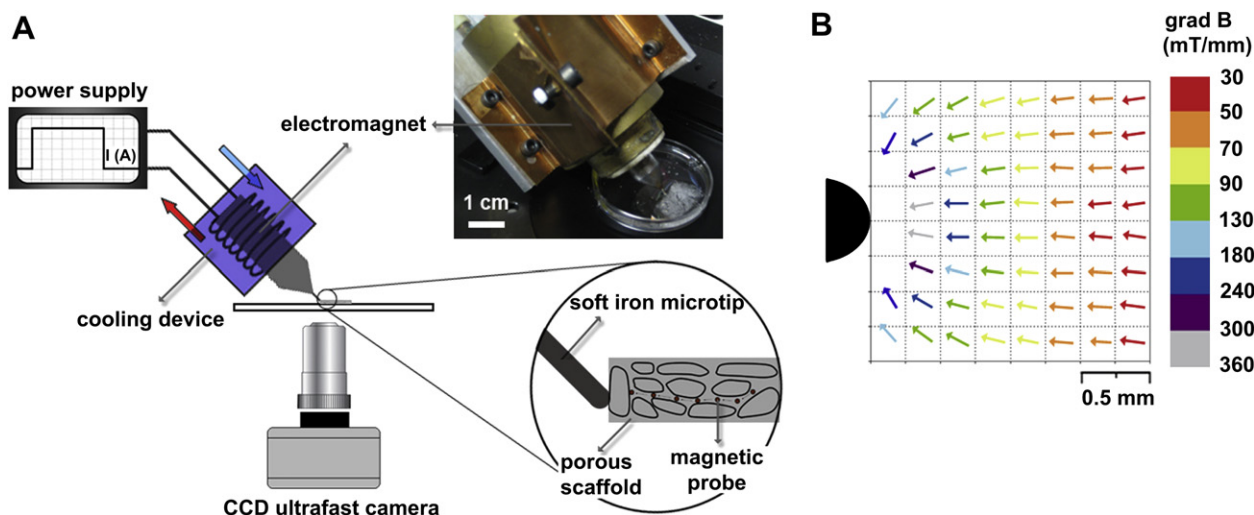


Fig. 1. A. Layout of a one pole magnetic tweezer. The magnet consists of a single coil enclosing a soft iron core. The core is needle shaped at the end, the magnetic flux is then bundled and the magnetic gradient reaches a maximum near the resulting 0.6 mm tip. A cooling system was included. The whole device is attached with a holder to a micro-manipulator placed on the microscope stage. The magnetic tip can then be positioned close to one scaffold extremity to perform mechanical measurement with magnetic probes. B. The magnetic field gradient generated by the tip was mapped on a $250 \mu\text{m} \times 250 \mu\text{m}$ grid by averaging the velocities of 20 single magnetic beads of known magnetization crossing each square. The resulting gradient and thus the force is directed to the tip and reaches 350 mT/mm at the tip proximity.

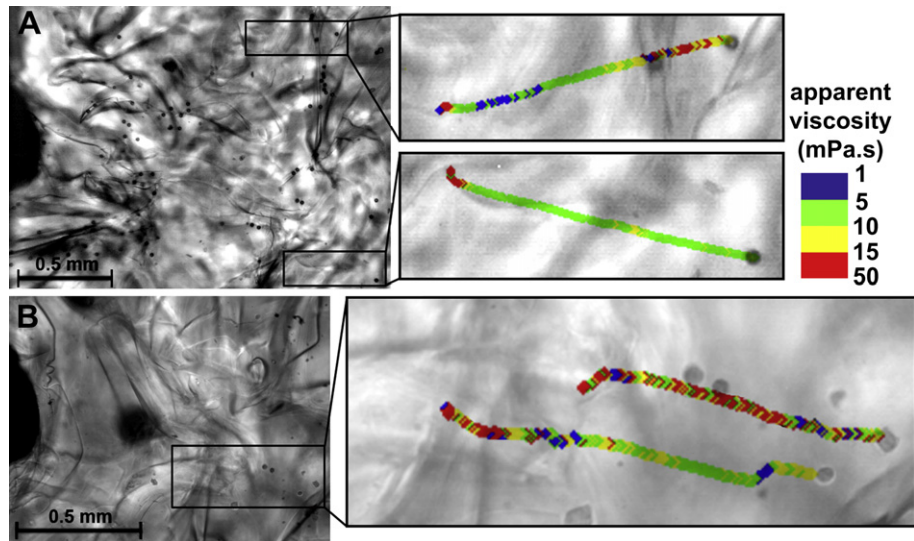


Fig. 2. Typical images of 18 μm magnetic beads (A) and magnetically labeled MSC (B) dispersed within the 3-D scaffold. The magnetic tip is clearly seen on the left. Trajectories of two individual magnetic beads and two individual MSC migrating due to the magnetic force, all tracked every 20 ms, in a rectangular zoomed part of the scaffold are superposed and colored according to their speed and therefore velocity. Color code is shown on the right in terms of mPa.s viscosity.

This article seeks to determine the physical attributes (local viscosity and stiffness) of a 3-D porous scaffold by applying a suite of microrheological measurements with different magnetic probes, either magnetic beads of varying sizes or magnetically labeled human stem cells. A magnetic tweezer system is described to apply controlled forces to a large number of beads or cells inside the scaffold. Finally, magnetic attraction was evaluated for its ability to optimize cell seeding in the construct and induce, through magnetic tweezers, a defined 3-D cellular organization.

2. Material and methods

2.1. Magnetic beads

Magnetic beads of 4.6 μm diameter and 18 μm diameter were purchased at Kisker. They consisted of a polystyrene matrix containing dispersed magnetite and were monodisperse in diameter. Their magnetic moments are given in Table 1. Magnetic beads of 100 μm diameter were custom-made by incorporation of maghemite nanoparticles into an alginate matrix using a single microemulsion method. They were polydisperse in size, with a diameter of $100 \pm 67 \mu\text{m}$, but exhibited a constant volume magnetization (see Table 1).

2.2. Magnetic cell labeling

Human Endothelial Progenitor Cells (EPC) isolated from cord blood were cultured at 37 $^{\circ}\text{C}$ and 5% CO_2 in endothelial basal medium-2 (EBM2) supplemented with EGM2-MV SingleQuots (Lonza). Human Mesenchymal Stem Cells (MSC) isolated from human bone marrow were cultured at 37 $^{\circ}\text{C}$ and 5% CO_2 in DMEM (Sigma) culture medium supplemented with 10% fetal calf serum, 1% penicillin/streptomycin and 1% glutamine. Both cell types are adherent during cell culture. In suspension, they are rounded with mean diameters of $13.8 \pm 2.1 \mu\text{m}$ for EPC and $18 \pm 4.2 \mu\text{m}$ for MSC.

The magnetic nanoparticles were synthesized following the Massart's method. They have a magnetic core made of maghemite ($\gamma\text{-Fe}_2\text{O}_3$) of 8 nm diameter and bear negative charges due to carboxylate groups on their surface, ensuring their stability in aqueous solution [42].

The cellular magnetic labeling [41,43] was performed by incubating a sterilized suspension of nanoparticles diluted in RPMI (Sigma) serum free culture medium supplemented with 5 mM citrate at a final iron concentration of 5 mM for 30 min. Incubation was followed by 1 h chase at 37 $^{\circ}\text{C}$ in nanoparticles free culture medium to ensure that all nanoparticles were internalized within the cells. Cells were then detached using trypsin (5 min at 37 $^{\circ}\text{C}$) and seeded on scaffolds. To obtain aggregates of EPC (mean diameter $80 \pm 14 \mu\text{m}$), cells were detached as patches by gentle pipetting after a short (30 s) incubation with trypsin.

Cell magnetizations were quantified using single-cell magnetophoresis, consisting in measuring the velocity of the magnetically labeled cells in suspension when submitted to a well-calibrated magnetic field gradient [44]. By balancing the

magnetic force with the viscous drag, one retrieves the magnetic moment of each single cell tracked and therefore the magnetic moment distribution over the cell population ($n = 200$).

2.3. Scaffolds

Polysaccharide-based scaffolds were prepared using a mixture of pullulan/dextran 75:25 with the cross-linking agent sodium trimetaphosphate (STMP) at 11% (w/v) under alkaline conditions (NaOH 10 M) [45–47]. Pores were created by a gas-foaming technique using sodium carbonate in 20% acetic acid solution. Scaffolds were freeze-dried for 48 h for complete removal of water and stored at room temperature until use. After hydration, scaffolds were transparent and maintained a regular internal lamellar pore structure, with porosity of 185–205 μm . Prior to cell seeding, the scaffolds were punched into discs having a cylindrical shape of 10 mm in diameter and 3 mm in thickness. Each sample was then seeded with 100 μl of a cell or bead suspension. For the viscosity measurements, probes were diluted at different concentrations prior to their seeding: 2×10^7 beads/ml for the 4.6- μm magnetic beads; 2×10^6 beads/ml for the 18- μm magnetic beads; 10^6 cells/ml for the magnetically labeled EPC and MSC cells. For the stiffness measurement, the 100- μm magnetic beads and the cell aggregates were seeded at 4×10^4 beads or aggregates per ml. For the magnetic cell confinement procedure, cells (4×10^5 cells/ml) were seeded under magnetic field application. To progressively degrade the scaffold, it was exposed to a mixture of pullulanase/dextranase (Sigma) and the stiffness was monitored every 20 s.

2.4. Magnetic tweezers

A magnetic tweezer is an electromagnetic device capable of exerting a force of controlled magnitude and direction on magnetic objects [48]. We developed a one-pole electromagnet consisting of a cylindrical soft iron core inserted in a coil connected to a power supply delivering current ranging from 0 to 4 A. The soft iron piece was tapered and polished to be ended as a sharp tip with diameter of 600 μm . The coil is alimented with a 2 A current, creating a 220 mT magnetic field at the tip proximity. A cooling system was necessary to avoid overheating and to prevent coil from melting. The magnetic tweezer system was mounted on a micromanipulator adapted to an optical inverted microscope. The tip contacted the sample with an incident angle of 45 $^{\circ}$. Bright-field images of the tip and magnetic probes in the samples were taken by an ultra-fast CCD camera at frame rates up to 60 Hz.

To magnetically modulate the cell organization inside the scaffold, the same soft iron material was machined to design small cylindrical tips (750 μm diameter) inserted in a non magnetic support and magnetized using a permanent magnet generating a 0.32 T magnetic field [49]. This micro-magnetic device was placed at the reverse side of the scaffolds seeded with magnetically labeled cells. As a control experiment, no magnet was placed.

The magnetic field gradients generated by the different tips were calibrated experimentally by tracking the velocity of individual magnetic beads of diameter $d = 4.6 \mu\text{m}$ diluted in a fluid of known viscosity. Magnetic force on the bead is counterbalanced by viscous force $3\pi\eta d v$ (Stokes law), where v is the bead velocity. In the region of interest, the magnetic field B is large enough (145 mT) so that M

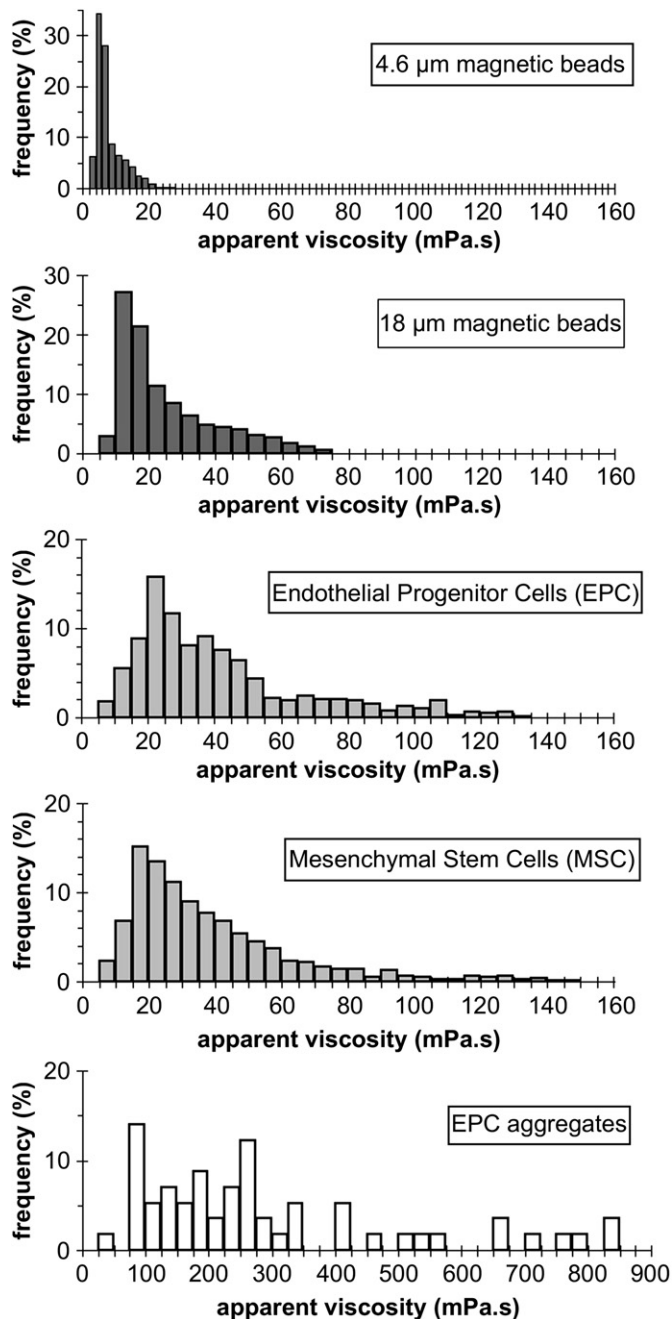


Fig. 3. Histograms of the apparent viscosities experienced by the magnetic probes and for a large number n of measures: magnetic beads of $4.6 \mu\text{m}$ ($n = 1056$) and $18 \mu\text{m}$ ($n = 4897$) diameter, magnetically labeled stem cells (EPC and MSC) of mean diameters $13.8 \mu\text{m}$ ($n = 987$) and $18 \mu\text{m}$ ($n = 2820$), respectively, and aggregates of EPC with diameters in the $80 \mu\text{m}$ range ($n = 58$).

reaches a saturable value M_{bead} and the magnetic force on each bead simply writes $M_{\text{bead}} \text{grad} B$. By tracking bead movement with a rapid camera (4 frames per second) and averaging the velocities of a large number of magnetic beads crossing sub-millimetric squares, the magnetic field gradient map was calculated for both tips.

2.5. Measure of the local apparent viscosity and stiffness

The magnetically induced motions of the probes (beads or cells) embedded in the scaffold were tracked and used to infer the scaffold rheological properties: internal viscosity and walls stiffness. The local apparent viscosity η_{app} was retrieved from the tracks of the probes displacements inside the construct when submitted to the magnetic force created by the tweezer. The probes velocities v_{probe} were computed from the measured displacement–time–data and were converted into viscosities using Stokes law $F_{\text{mag}} = 3\pi\eta_{\text{app}}d_{\text{probe}}v_{\text{probe}}$, where F_{mag} is the local magnetic force component parallel

to the probe's displacement. The stiffness of the scaffold internal walls could be measured when a magnetic probe was pressed on a pore wall. The movement of such a probe embedded in the wall was tracked during repeated force on–off cycles, each on or off phase lasting a few seconds. The instantaneous elastic response corresponds to a jump Δd in the displacement and allows retrieving the elastic modulus G (expressed in Pa), named stiffness in the following, as $F = 3\pi G d_{\text{probe}} \Delta d$.

3. Results

3.1. Magnetic field gradient and forces experienced by magnetic probes

This study first reports the design and characterization of a magnetic tweezer (Fig. 1) that enables to maneuver small magnetic probes inside a 3-D scaffold. To calibrate the magnetic field gradient generated by the thin tip, $4.6 \mu\text{m}$ diameter magnetic beads were tracked near the tip in a liquid of known viscosity and the bead velocities were converted into force (and thereby magnetic field gradients) using a classic viscous drag approach (Stokes law). The mapping of the magnetic field gradient (in 0.25 mm squares) is presented in Fig. 1. The magnetic field gradient is inhomogeneous, increasing when approaching the tip. The tip dimension (tenth of mm) allowed achieving forces over a large millimetric area. Table 1 presents the different probes used in terms of diameter and magnetization. The magnetic field gradient is then converted into force, which reach a maximum value near the tip (given for each probe in Table 1). The force applied to the probes at a 1 mm distance from the tip is given as well in Table 1. Forces of almost $2 \mu\text{N}$ on the largest $100 \mu\text{m}$ magnetic beads were reached near the tip. For smaller $18 \mu\text{m}$ -beads or magnetic cells, the force was in the 200 – 1000 pN range near the tip, and fell to tens of pN at 1 mm from the tip.

3.2. Magnetic migration of beads and cells inside the porous scaffold

The magnetic beads or magnetically labeled cells seeded were homogeneously distributed in the microarchitecture of the transparent scaffold (see large views in Fig. 2) and each probe could be imaged individually. Upon the application of the magnetic field gradient, the magnetic probes are driven into movement, towards the magnetic tip. First, this demonstrates the magnetic mobility of small magnetic objects, including magnetically labeled cells, in the internal structure of a porous scaffold. Second, the local viscosity could be explored by tracking the driven motion of the probes (see Fig. 2 for typical trajectories).

3.3. Apparent viscosities

The internal viscosity of the scaffold governs the seeding of cells or particles inside the construct. The viscosity was measured using magnetic beads of two different diameters ($4.6 \mu\text{m}$ and $18 \mu\text{m}$), two types of magnetically labeled stem cells (EPC and MSC), and aggregates of EPC. For each probe type submitted to the magnetic tweezer, hundreds of local velocities were collected and converted into local viscosities. The obtained values are apparent viscosities and reflect the viscosity of each probe environment and differ from probe to probe. Histograms of the apparent viscosities are presented in Fig. 3. The viscosities always display a large distribution which is due to local structural variations at the scaffold microscale. The scaffold lamellar pores, into which small objects can migrate to colonize the construct, are therefore inhomogeneous regarding to their internal viscosity. Moreover, the average value of the apparent viscosities is probe dependent. For magnetic beads, the viscosity felt by the $18 \mu\text{m}$ -beads is nearly four times higher than the one obtained in the $4.6 \mu\text{m}$ -beads vicinity. The apparent viscosity

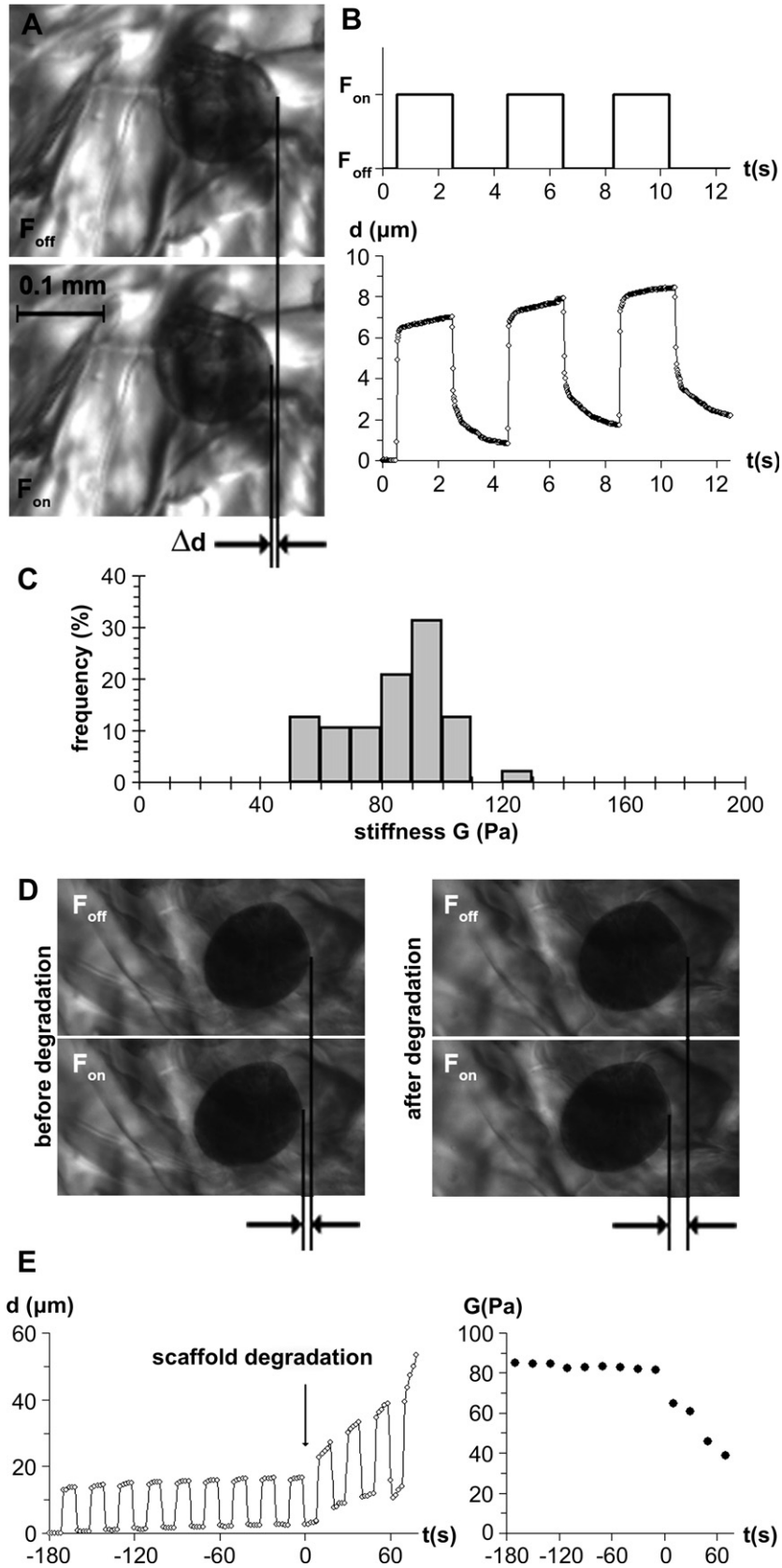


Fig. 4. Stiffness of the scaffold internal walls probed with 100 μm magnetic beads. **A.** Images of a magnetic bead oscillation when moving against a wall. The two black vertical lines denote the initial elastic jump Δd of the bead. The 130 μm diameter bead is located 1 mm far from the magnetic tip, and experiences a 62 mT/mm magnetic field gradient, corresponding to a 685 nN magnetic force when the field is turned on. **B.** Tracked displacement of the bead during the repeated application of 2 s magnetic force pulses. The strongly elastic nature of the scaffold walls is clearly observed by the jump upon turning on the magnetic field and the relaxation upon turning off. For the considered bead, the local stiffness found is $G = 96.8 \pm 1.6$ Pa. **C.** Histograms of the retrieved stiffness G (expressed in Pa) for 48 measurements. **D.** Images of another magnetic bead oscillation, in an intact scaffold (left) and after soft scaffold degradation (right). The elastic jump Δd , denoted by the vertical lines, increases after the degradation treatment. **E.** Corresponding bead displacements before and after the scaffold degradation (left) and resulting stiffness G (right).

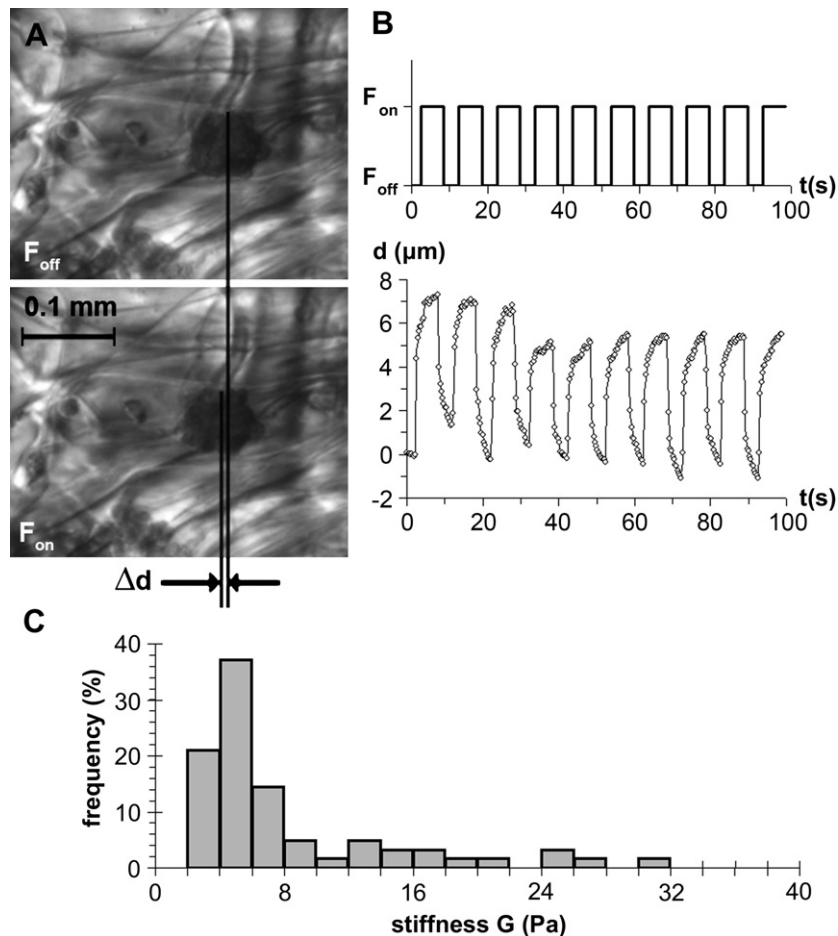


Fig. 5. Stiffness of the scaffolds internal walls probed with 80 μm magnetic EPC aggregates. A. Sequences of two images showing the aggregate oscillation when moving against a wall. The 71 μm diameter aggregate is located 0.5 mm far from the magnetic tip, and experiences a 142 mT/mm magnetic field gradient, corresponding to a 13 nN magnetic force when the field is turned on. The two black vertical lines denote the initial elastic jump Δd of the aggregate. B. Tracked displacement of the aggregate during the repeated applications of 6 s magnetic forces pulses. For the considered aggregate, the local stiffness found is $G = 4.8 \pm 0.4$ Pa. C. Histograms of the retrieved stiffness G (expressed in Pa) for 62 measurements.

displayed around the 18 μm -cells (MSC) is larger by a factor 1.7 than the one obtained with the 18 μm -beads while having the same diameter. Finally, the viscosity measurements performed with smaller 13.8- μm -EPC cells revealed a slight viscosity decrease (factor 1.3) compared with the 18 μm -MSC cells. However, for three probes with diameter in the 10 μm range (18 μm -beads, MSC and EPC cells), the changes in viscosities are not statistically different. The three probes therefore seem to sense the same microenvironment. In sharp contrast, the apparent viscosity probed with the 80 μm -aggregates of cells is found ten times higher than the one obtained with individual cells. This analysis shows a clear tendency for an increase of the internal apparent viscosity with the size of the objects colonizing the scaffold.

3.4. Stiffness of the scaffold walls probed by magnetic beads and magnetic cells aggregates

The stiffness of the wall is one of the major determinants for cell adhesion and migration in scaffolds. We used large 100 μm -beads or 80 μm -aggregates of cells that were adjacent to the pore walls and subjected to repeated applications of a few seconds magnetic force pulses. Fig. 4A and B shows the displacement of a magnetic bead after the application of the force pulses. The response curve (Fig. 4B) exhibits an initial elastic regime, defined as the instantaneous jump in displacement. The stiffness G (expressed in Pa) is then directly

retrieved from the jump. It is distributed between 50 and 130 Pa (Fig. 4C), with an average of 70.8 Pa and a standard deviation of 15.1 Pa. To test the sensitivity of the measure regarding to the scaffold intrinsic properties, we measured the stiffness after a soft treatment of the scaffold with a degrading agent (Fig. 4D and E). Within the first minute after addition of the degrading enzyme, it appeared clearly that the stiffness was lowered.

As a second step, we probed the stiffness of the internal walls with aggregates of magnetically labeled cells (EPC) of average diameter 80 μm . Typical displacements in response to force pulses are shown in Fig. 5A and B and resulting stiffness is shown in Fig. 5C. The value is peaked around 5 Pa, with an average value of 8.4 Pa, eight times lower than the stiffness experienced by the 100 μm -beads. This is likely to be due to a deformability of the cell aggregates, which tend to adopt the wall microarchitecture.

3.5. Local magnetic confinement of stem cells inside the porous scaffold

Tips of similar dimension and magnetization than the one used for the previous magnetic micro-manipulations were disposed in a hexagonal array (Fig. 6A). They were magnetized at saturation using a permanent magnet and developed a magnetic field gradient 5 times higher than the one created by the tip inserted in the

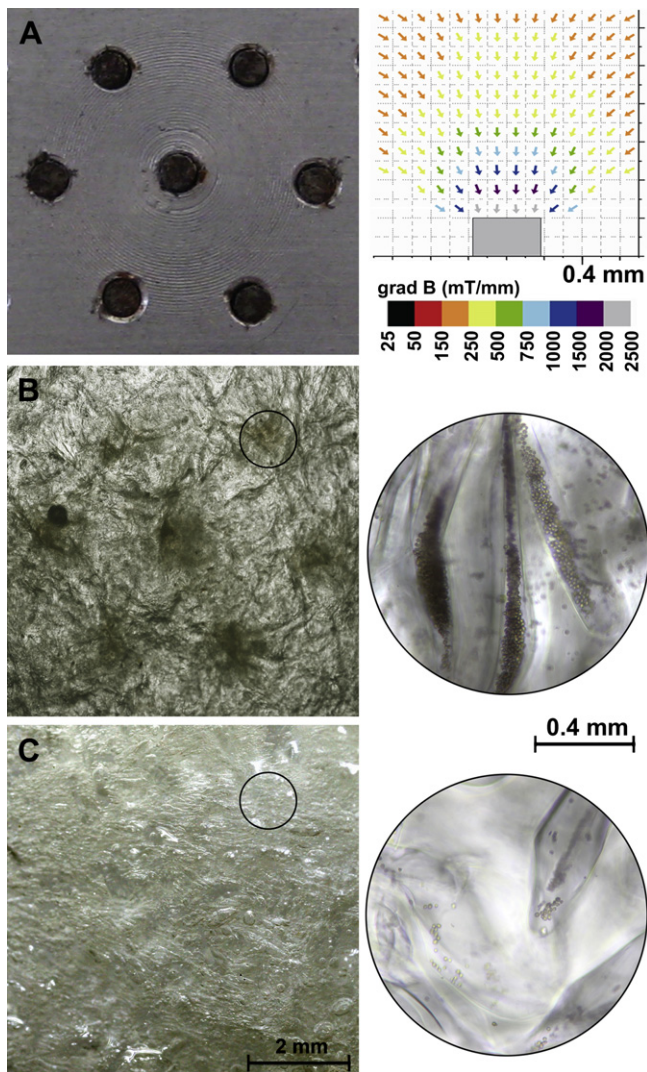


Fig. 6. Modulation of the cell organization within the scaffolds. A. (left): A hexagonal array of 0.75 mm diameter cylindrical tips similar to the one described in Fig. 1 is magnetized and placed at the reverse side of the scaffold, before cell seeding on the top of the scaffold. (right): The magnetic field gradient created by each cylindrical tip is mapped on a grid of $200\ \mu\text{m} \times 200\ \mu\text{m}$ by averaging the velocities of 40 single magnetic beads crossing each square. At the tip proximity, the magnetic field gradient is close to 2000 mT/mm B. (left): Photographic image of a scaffold seeded with 4×10^5 magnetic MSC cells, under the influence of the magnetic fields created by the tips, demonstrating the precise cell patterning formation of hexagonal multicellular assemblies within the scaffold. (right): Magnification by $10\times$ of the reported circle area of the scaffold at one site of the magnetic attraction, showing an impressive confinement of the MSC cells inside the scaffold pores, with hundreds of cells in each pore. C. (left): Photographic image of a scaffold seeded with 4×10^5 magnetic MSC without magnet application on the tips. No cellular organization was observed. (right): Zoomed observation using $10\times$ magnification within the circle area. The cells are homogeneously distributed within all scaffold pores with only about ten cells in each pore.

electromagnet. Focalized magnetic forces were thus generated by these submillimetric tips placed at the reverse side of a scaffold. The same hexagonal pattern was successfully achieved inside the scaffold with the magnetic MSC (Fig. 6B), evidencing a cellular confinement at the vicinity of the micro-magnets. This confinement was clearly observable inside the scaffolds pores, where MSC appeared densely packed (Fig. 6B, right panel). At the opposite, for the control situation where the same numbers of magnetic cells were seeded without magnetization of the tips, no cell organization was visible on large scaffolds views (Fig. 6C) and only few cells were present inside the pores (Fig. 6C, right panel). We measured the

average number of cells per mm^2 inside the pores and found 2735 ± 630 cells/ mm^2 for the magnetic assisted seeding and 210 ± 85 cells/ mm^2 for the control seeding, leading to 10 times enhancement in cell confinement. Therefore, the magnetic force-assisted cell seeding presented here was sufficient to confine cells into the scaffolds and to force a multicellular organization.

4. Discussion

4.1. Magnetic micro-manipulations to investigate physical properties of porous scaffolds

Most of the scaffolds used in tissue engineering are porous and degradable structures. They are fabricated using various natural and synthetic materials and present complex internal structures with intricate pores and channels. The cell colonization of each scaffold is a common goal. Here, we used hydrogel scaffolds with lamellar architecture prepared from naturally-derived polysaccharides, recently developed and evaluated as novel efficient scaffolds for in vitro and in vivo tissue reconstruction [50–52]. The presented technique can be extended to any type of porous, transparent, and soft scaffold.

Cell seeding inside the scaffold pores and cell attachment to the pore walls are the first steps determining cell colonization of the scaffold and subsequent tissue formation. The properties controlling these events must be carefully evaluated during the development of scaffolds. While the cell infiltration inside the scaffolds can be determined by the viscous drag resisting the cell movement, the cell adhesion is related to the stiffness of the internal walls. Local differences in these mechanical properties will not be detected by bulk measurements such as tensile tests, compressive tests, or DMA. Developing innovative tools to explore the local viscosity and stiffness at the microscale should therefore become crucial to the design of scaffolds. Microrheometric techniques have become a major tool for investigating mechanical properties of complex soft materials. Magnetic methods should be preferred over other techniques because magnetic gradients can be applied to multiple magnetic particles over large distances (of a few mm), and with large forces. It is then possible, within the same field of view, to probe single micrometric objects at various locations and therefore to mechanically “map” distinct regions. This is of particular importance for the study of the cells microenvironment in 3-D scaffolds as cells will respond to the scaffolds spatial variations in physical properties in the order of microns. Here, we are among the first to apply magnetic micro-rheometry to 3-D porous scaffolds.

We developed a magnetic tweezer with one pole microtip, having large diameter (600 μm), to allow the magnetic force application over a large area of (few mm). For 18 μm magnetic beads, the force attained 300 pN at 1 mm from the tip, in the relevant range to control the magnetic migration of micro-objects inside the scaffolds channels. Using 100 μm magnetic beads, the force was 1000-fold higher (310 pN at 1 mm from the tip) and was sufficient to deform the pore walls and retrieve their stiffness. Besides, we also used human stem cells, magnetically labeled with iron oxide magnetic nanoparticles, as biological magnetic probes. Previous works have already demonstrated the preservation of cell viability, cell phenotype and cell functions after magnetic labeling [41]. The magnetic stem cells act both as probes that can be maneuvered with external magnetic fields to infer the mechanical properties of their surrounding microenvironment, and as future actors of the scaffold cell colonization towards tissue regeneration. This approach using cell probes to retrieve their own microenvironmental features is particularly novel and biologically relevant.

4.2. Apparent viscosity in the scaffold pores

The contribution of hydrodynamic environment for the cell seeding, expressed as the local viscosity was investigated. This parameter allows to evaluate the seeding efficiency of a given scaffold. First, it is noteworthy that, while small 4.6 μm -beads experience a lower viscosity of about 6 mPa s, beads or cells of diameter in the range 14–18 μm suffer approximately the same viscosity, in between 20 and 35 mPa s, demonstrating the accuracy of the measure. Second, the viscosity in the environment of aggregates containing a few cells reveals a marked increase to 280 mPa s in average. The viscosity measured is named apparent viscosity as it includes not only the aqueous solution (which should equal the 1 mPa s viscosity of water) but also some frictions onto the channels walls. A larger probe is more susceptible to be slowed down by obstacles and its apparent viscosity to be larger. This is clearly demonstrated by the measurements performed here with 5 types of probes of different diameters.

The apparent viscosity value for a given cell type then allows modulating the corresponding cell seeding duration. In particular, the conventional method of incorporating cells into scaffolds is passive, i.e. by gravity, and the cells are simply brought into direct contact to the scaffolds top. Assuming a cell density of 1.2 kg/m^3 , the seeding duration for the cells to penetrate over 1 mm inside the scaffolds investigated here is about 10 min. Another method is to force the cell seeding in a bioreactor, where a centrifugal force, in the order of a few g (15–30 rpm), facilitates the transfer of cells inside the scaffold [53]. The time duration is then shortened by a factor that is directly the number of g of the centrifugal acceleration. In the present case, if the cells were to be magnetized, the mean velocity in the scaffold internal channels is close to 20 $\mu\text{m}/\text{s}$ for a magnetic field gradient no higher than 50 mT/mm, which means that a seeding duration of a few tens of seconds would be long enough for the cells to move across the 1 mm distance. Finally, if one considers seeding aggregates under gravitational force, the seeding through 1 mm is taking more than two hours. Aggregates therefore move much slower than single cells and this must be taken into account when estimating the attracting advantage to seed already aggregated stem cells to enhance tissue formation [13].

4.3. Local determination of the scaffold stiffness at the cellular scale

We successfully retrieved the local stiffness of the scaffold walls at the microscale using 100 μm -sized embedded beads oscillated by the magnetic tweezer. The stiffness is found in the 50 Pa range. For a bead submitted to a 50 mT/mm magnetic gradient, the elastic jump in between 5 and 10 μm is easily detectable. Using a higher spatial magnification (20 \times) allowing submicrometer spatial sensitivity and tracking beads closer to the tip (in the 300 mT/mm range), one could accurately measure stiffness in the kPa range. Besides, thinner magnetic tips could be adapted to develop gradients of 2000 mT/mm close to the tip, larger magnetic beads could be fabricated (a doubling of the bead diameter leads to a 8 times increase for the bead magnetic moment) and walls as stiff as 100 kPa could be probed. Therefore, magnetic bead micro-rheometry inside a 3-D scaffold could be used to infer the internal walls stiffness in the 1 Pa–100 kPa range, which is appropriate for the cell adhesion and differentiation processes. Indeed, endothelial progenitors (EPC) differentiate and form tubular structures on a Matrigel, a biological soft matrix (50 Pa stiffness range) [54]. Moreover, the influence of the physical and chemical properties of the cellular microenvironment on stem cell differentiation has recently been considered. The relative stiffness of a substrate can orient cell differentiation, without the need for specific growth

factors. Thus, adult neuronal stem cells differentiation into neurons was favored by soft (<1 kPa) surfaces [55]. Similarly, a soft substrate with a stiffness similar to that of the brain (1 kPa) orients MSC differentiation into neuronal cells, while a hard substrate comparable to bone tissue (100 kPa) gives rise to bone cells, and an intermediate substrate (10 kPa) to muscle cells [19]. These results, obtained with 2-D substrates, have important implications for the design of stem cell supportive matrices. A scaffold with a certain local stiffness could promote pre-differentiation before stem cell implantation into an injured organ, in situations where the altered host microenvironment can no longer induce appropriate differentiation. To conclude, the evaluation of the scaffolds stiffness at the cellular level should become more important in tissue engineering approaches.

4.4. Magnetic force-assisted cell seeding

Cell seeding is the main step in constructing the tissue-like structure in 3-D scaffolds. Obviously, any technique likely to enhance the initial step of cell seeding could be highly valuable. Here, we demonstrate that magnetic force-assisted cell seeding provide an effective and high-density cell seeding into 3-D scaffolds. Moreover, we demonstrate that, using magnetic microtips developing high magnetic forces, we could achieve a precise spatial cellular organization inside the scaffold. Magnetic seeding has been obtained very recently using cells labeled with magnetic cationic liposomes and an external permanent magnet placed at the reverse side of a scaffold during seeding [14]. This novel cell seeding methodology led to a cell seeding efficiency that was 3-fold higher than conventional passive seeding, in a homogeneous fashion. Here the use of focalized magnetic fields together with high magnetic field gradients allowed to confine cells inside the scaffold pores at a density more than 10-fold the one obtained for static seeding. Cells are tightly held together into the pores. To achieve such a confinement, the only other alternative was to seed cells as aggregates. However, as previously demonstrated hereby, cell aggregates could be difficult to seed into 3-D scaffolds, due to hydrodynamic constraints. In this work, seeding is achieved with cells that are further packed together when reaching their final location within the pores. This takes on a strategic importance in the context for instance of cartilage tissue engineering involving the chondrogenesis of mesenchymal stem cells (MSC) in the 3-D scaffolds. Indeed, cartilage formation requires the cells to be confined in a 3-D aggregate composed of several hundred thousand cells. The confined cellular organization presented here is currently being tested to promote chondrogenesis in these 3-D scaffolds, which has not yet been reported. As the magnetic seeding is associated with the stem cell labeling with magnetic nanoparticles, the impact of the magnetic label to the differentiation process has to be evaluated concomitantly (work in progress).

5. Conclusions

This study illustrates a methodology for the systematic investigation of the internal local physical properties of 3-D scaffolds. The magnetic tweezer set-up provides forces controllable in amplitude and direction to maneuver magnetic probes (beads or cells) inside the scaffolds, allowing an accurate measurement of the apparent viscosity of the internal channels and the stiffness of the pores walls. The viscosity inside the scaffolds channels is a key influencer in the outcome of cell seeding duration and efficiency and is found to be highly dependent on the material seeded. In particular, individual cells are found to experience a viscosity ten times lower than small aggregates of cells which will therefore seed much slower. The substrate stiffness has recently emerged to

template the cells migration and differentiation. The local stiffness retrieved here is in the 50 Pa range but stiffness up to 100 kPa could be accessed through the magnetic micro-rheometry. The determination of these local mechanical properties will be crucial to the design of scaffolds, for stem cells colonization and differentiation. Moreover, it is demonstrated here that cells can be confined in the scaffold to achieve high cellular density, and that the cell distribution can be modulated by an array of micro-magnetic tips. This multidisciplinary approach for tissue engineering combines magnetic cell labeling based on nanotechnology, magnetic field miniaturization to develop high magnetic field gradient, micro-rheometry and biology of stem cells. The microrheological methodology will be essential to develop implantable tissue substitutes that can provide the appropriate mechanical cues to the cells. Future work should focus on the way cells interact with scaffolds in relation with their mechanical environment. Besides, the initial mechanical properties of biomaterials are not the only factors decisive for the cellular fate: over time, the substrate mechanics may undergo significant change due to degradation of the matrix and/or the deposition of macromolecules and these changes would need to be locally probed and monitored.

Acknowledgements

We thank Nathalie Luciani and Jean-Claude Bacri for fruitful discussions. This work was supported by the grants from the French national research agency, ANR-PCV "3D MIGMAG" and ANR TEC-SAN "ITOV".

Appendix

Figures with essential color discrimination. Certain figures in this article, in particular Figs. 1, 2 and 6 may be difficult to interpret in black and white. The full color images can be found in the on-line version, at doi:10.1016/j.biomaterials.2009.11.014.

References

- Griffith LG, Naughton G. Tissue engineering—current challenges and expanding opportunities. *Science* 2002;295(5557):1009–14.
- Vunjak-Novakovic G, Radisic M. Cell seeding of polymer scaffolds. *Methods Mol Biol* 2004;238:131–46.
- Fromstein JD, Zandstra PW, Alperin C, Rockwood D, Rabolt JF, Woodhouse KA. Seeding bioreactor-produced embryonic stem cell-derived cardiomyocytes on different porous, degradable, polyurethane scaffolds reveals the effect of scaffold architecture on cell morphology. *Tissue Eng Part A* 2008;14(3):369–78.
- Guillot PV, Cui W, Fisk NM, Polak DJ. Stem cell differentiation and expansion for clinical applications of tissue engineering. *J Cell Mol Med* 2007;11(5):935–44.
- Lawrence BJ, Madhally SV. Cell colonization in degradable 3D porous matrices. *Cell Adh Migr* 2008;2(1):9–16.
- Schliephake H, Zghoul N, Jager V, van Griensven M, Zeichen J, Gelinsky M, et al. Effect of seeding technique and scaffold material on bone formation in tissue-engineered constructs. *J Biomed Mater Res A* 2009;90(2):429–37.
- Zehbe R, Libera J, Gross U, Schubert H. Short-term human chondrocyte culturing on oriented collagen coated gelatin scaffolds for cartilage replacement. *Biomed Mater Eng* 2005;15(6):445–54.
- Li Y, Ma T, Kniss DA, Lasky LC, Yang ST. Effects of filtration seeding on cell density, spatial distribution, and proliferation in nonwoven fibrous matrices. *Biotechnol Prog* 2001;17(5):935–44.
- Kitagawa T, Yamaoka T, Iwase R, Murakami A. Three-dimensional cell seeding and growth in radial-flow perfusion bioreactor for in vitro tissue reconstruction. *Biotechnol Bioeng* 2006;93(5):947–54.
- Bueno EM, Bilgen B, Barabino GA. Wavy-walled bioreactor supports increased cell proliferation and matrix deposition in engineered cartilage constructs. *Tissue Eng* 2005;11(11–12):1699–709.
- Martin I, Wendt D, Heberer M. The role of bioreactors in tissue engineering. *Trends Biotechnol* 2004;22(2):80–6.
- Godbey WT, Hindy SB, Sherman ME, Atala A. A novel use of centrifugal force for cell seeding into porous scaffolds. *Biomaterials* 2004;25(14):2799–805.
- Anil Kumar PR, Varma HK, Kumary TV. Cell patch seeding and functional analysis of cellularized scaffolds for tissue engineering. *Biomed Mater* 2007;2(1):48–54.
- Shimizu K, Ito A, Honda H. Enhanced cell-seeding into 3D porous scaffolds by use of magnetic nanoparticles. *J Biomed Mater Res B Appl Biomater* 2006;77(2):265–72.
- Shimizu K, Ito A, Honda H. Mag-seeding of rat bone marrow stromal cells into porous hydroxyapatite scaffolds for bone tissue engineering. *J Biosci Bioeng* 2007;104(3):171–7.
- Chai C, Leong KW. Biomaterials approach to expand and direct differentiation of stem cells. *Mol Ther* 2007;15(3):467–80.
- Saha K, Pollock JF, Schaffer DV, Healy KE. Designing synthetic materials to control stem cell phenotype. *Curr Opin Chem Biol* 2007;11(4):381–7.
- Curran JM, Chen R, Hunt JA. The guidance of human mesenchymal stem cell differentiation in vitro by controlled modifications to the cell substrate. *Biomaterials* 2006;27(27):4783–93.
- Engler AJ, Sen S, Sweeney HL, Discher DE. Matrix elasticity directs stem cell lineage specification. *Cell* 2006;126(4):677–89.
- Wang JH, Thampatty BP. Mechanobiology of adult and stem cells. *Int Rev Cell Mol Biol* 2008;271:301–46.
- Kniazeva E, Putnam AJ. Endothelial cell traction and ECM density influence both capillary morphogenesis and maintenance in 3-D. *Am J Physiol Cell Physiol* 2009;297(1):C179–87.
- Peyton SR, Kim PD, Ghajar CM, Selihtar D, Putnam AJ. The effects of matrix stiffness and RhoA on the phenotypic plasticity of smooth muscle cells in a 3-D biosynthetic hydrogel system. *Biomaterials* 2008;29(17):2597–607.
- Gwak SJ, Bhang SH, Kim IK, Kim SS, Cho SW, Jeon O, et al. The effect of cyclic strain on embryonic stem cell-derived cardiomyocytes. *Biomaterials* 2008;29(7):844–56.
- Brandl F, Sommer F, Goepferich A. Rational design of hydrogels for tissue engineering: impact of physical factors on cell behavior. *Biomaterials* 2007;28(2):134–46.
- Dado D, Levenberg S. Cell-scaffold mechanical interplay within engineered tissue. *Semin Cell Dev Biol* 2009;20(6):656–64.
- Jancar J, Slovickova A, Amler E, Krupa P, Kecova H, Planka L, et al. Mechanical response of porous scaffolds for cartilage engineering. *Physiol Res* 2007;56(Suppl. 1):S17–25.
- Lin AS, Barrows TH, Cartmell SH, Guldberg RE. Microarchitectural and mechanical characterization of oriented porous polymer scaffolds. *Biomaterials* 2003;24(3):481–9.
- Anseth KS, Bowman CN, Brannon-Peppas L. Mechanical properties of hydrogels and their experimental determination. *Biomaterials* 1996;17(17):1647–57.
- Vinckier A, Semenza G. Measuring elasticity of biological materials by atomic force microscopy. *FEBS Lett* 1998;430(1–2):12–6.
- Koenders MM, Yang L, Wismans RG, van der Werf KO, Reinhardt DP, Daamen W, et al. Microscale mechanical properties of single elastic fibers: the role of fibrillin-microfibrils. *Biomaterials* 2009;30(13):2425–32.
- Manduca A, Oliphant TE, Dresner MA, Mahowald JL, Kruse SA, Amromin E, et al. Magnetic resonance elastography: non-invasive mapping of tissue elasticity. *Med Image Anal* 2001;5(4):237–54.
- Othman SF, Xu H, Royston TJ, Magin RL. Microscopic magnetic resonance elastography (microMRE). *Magn Reson Med* 2005;54(3):605–15.
- Waigh T. Microrheology of complex fluids. *Rep Prog Phys* 2005;68:685–742.
- Wilhelm C, Browaeys J, Ponton A, Bacri JC. Rotational magnetic particles microrheology: the Maxwellian case. *Phys Rev E Stat Nonlin Soft Matter Phys* 2003;67(1 Pt 1):011504.
- Leung LY, Tian D, Brangwynne CP, Weitz DA, Tschumperlin DJ. A new microrheometric approach reveals individual and cooperative roles for TGF-beta1 and IL-1beta in fibroblast-mediated stiffening of collagen gels. *FASEB J* 2007;21(9):2064–73.
- Velegol D, Lanni F. Cell traction forces on soft biomaterials. I. Microrheology of type I collagen gels. *Biophys J* 2001;81(3):1786–92.
- Wilhelm C. Out-of-equilibrium microrheology inside living cells. *Phys Rev Lett* 2008;101(2):028101.
- Balland M, Desprat N, Icard D, Fereol S, Asnacios A, Browaeys J, et al. Power laws in microrheology experiments on living cells: comparative analysis and modeling. *Phys Rev E Stat Nonlin Soft Matter Phys* 2006;74(2 Pt 1):021911.
- Kuo SC. Using optics to measure biological forces and mechanics. *Traffic* 2001;2(11):757–63.
- Marion S, Wilhelm C, Voigt H, Bacri JC, Guillen N. Overexpression of myosin IB in living *Entamoeba histolytica* enhances cytoplasm viscosity and reduces phagocytosis. *J Cell Sci* 2004;117(Pt 15):3271–9.
- Wilhelm C, Gazeau F. Universal cell labelling with anionic magnetic nanoparticles. *Biomaterials* 2008;29(22):3161–74.
- Wilhelm C, Gazeau F, Roger J, Pons JN, Salis MF, Perzynski R, et al. Binding of biological effectors on magnetic nanoparticles measured by a magnetically induced transient birefringence experiment. *Phys Rev E Stat Nonlin Soft Matter Phys* 2002;65(3 Pt 1):031404.
- Wilhelm C, Bal L, Smirnov P, Galy-Fauroux I, Clement O, Gazeau F, et al. Magnetic control of vascular network formation with magnetically labeled endothelial progenitor cells. *Biomaterials* 2007;28(26):3797–806.
- Wilhelm C, Gazeau F, Bacri JC. Magnetophoresis and ferromagnetic resonance of magnetically labeled cells. *Eur Biophys J* 2002;31(2):118–25.
- Autissier A, Letourneur D, Le Visage C. Pullulan-based hydrogel for smooth muscle cell culture. *J Biomed Mater Res A* 2007;82(2):336–42.

- [46] Le Visage C, Chaubet F, Autissier A, Letourneur D. Method for preparing porous scaffold for tissue engineering. EP Patent application 07301451.6-1219; 2008.
- [47] Poirier-Quinot M, Frasca G, Wilhelm C, Luciani N, Ginefri JC, Darrasse L, et al. High resolution 1.5 T magnetic resonance imaging for tissue engineering constructs: a non invasive tool to assess 3D scaffold architecture and cell seeding. *Tissue Eng Part C Methods* 2009.
- [48] Kollmannsberger P, Fabry B. High-force magnetic tweezers with force feedback for biological applications. *Rev Sci Instrum* 2007;78(11):114301.
- [49] Frasca G, Gazeau F, Wilhelm C. Formation of a three-dimensional multicellular assembly using magnetic patterning. *Langmuir* 2009;25(4):2348–54.
- [50] Chaouat M, Le Visage C, Autissier A, Chaubet F, Letourneur D. The evaluation of a small-diameter polysaccharide-based arterial graft in rats. *Biomaterials* 2006;27(32):5546–53.
- [51] Derkaoui SM, Avramoglou T, Barbaud C, Letourneur D. Synthesis and characterization of a new polysaccharide-graft-polymethacrylate copolymer for three-dimensional hybrid hydrogels. *Biomacromolecules* 2008;9(11):3033–8.
- [52] Abed A, Deval B, Assoul N, Bataille I, Portes P, Louedec L, et al. A biocompatible polysaccharide hydrogel-embedded polypropylene mesh for enhanced tissue integration in rats. *Tissue Eng Part A* 2008;14(4):519–27.
- [53] Li WJ, Jiang YJ, Tuan RS. Cell-nanofiber-based cartilage tissue engineering using improved cell seeding, growth factor, and bioreactor technologies. *Tissue Eng Part A* 2008;14(5):639–48.
- [54] Spencer NJ, Cotanche DA, Klapperich CM. Peptide- and collagen-based hydrogel substrates for in vitro culture of chick cochleae. *Biomaterials* 2008;29(8):1028–42.
- [55] Leipzig ND, Shoichet MS. The effect of substrate stiffness on adult neural stem cell behavior. *Biomaterials* 2009.